An improved key-phase-free blade tip-timing technique for nonstationary test conditions and its application on large-scale centrifugal compressor blades

An improved key-phase-free blade tip-timing technique for nonstationary test conditions and its application on large-scale centrifugal compressor blades

Changbo He, Jerome Antoni, Alessandro Paolo Daga, Hongkun Li, Ning Chu, Siliang Lu, Zhixiong Li

Abstract **- Large-scale centrifugal compressor is an essential fluid machinery in modern industry. The blades, a critical part of compressors, always work under severe and harsh conditions and are prone to fatigue failure. Thus, a suitable monitoring technique is necessary to guarantee reliable operation of blades on the long-term. One promising, non-contact, online, technique, is the blade tip-timing (BTT) which is able to recover the vibration characteristics of all the blades simultaneously. However, improvements are still necessary to ensure the accuracy and reliability of the BTT technique for vibration monitoring of large-scale centrifugal compressors. In this paper, the resolution error induced by the finite, discrete sampling is studied first. Then, the experimental random errors brought by nonstationary operating conditions are analyzed in detail and the error introduced by the compensation of the geometrical imperfection of the blades is also taken into account. An improved technique is proposed to reduce such random errors by substituting the real key-phase signal with a reconstruction by means of the tip-timing signal. Experiment on a centrifugal compressor test-rig with a cracked blade is conducted to verify the effectiveness of the improved technique. Finally, a dynamic model is built to support the experimental result. This work demonstrates the reliability of the improved BTT technique for blade condition monitoring and fault warning of large-scale centrifugal compressors.**

Index Terms **- Centrifugal compressor, Improved blade tip-timing, BTT, Blade crack, Dynamic analysis**

This work was supported by Natural Science Foundation of China under Grant No. U1808214 and China Scholarship Council (No. 201706060161) (corresponding author: Hongkun Li)

Changbo He is with the College of Electrical Engineering and Automation, Anhui University, Hefei 230601, China and Laboratoire Vibrations Acoustique, INSA-Lyon, LVA EA677, F-69621 Villeurbanne, France. (email: changbh@ahu.edu.cn)

Jerome Antoni is with the Laboratoire Vibrations Acoustique, INSA-Lyon, LVA EA677, F-69621 Villeurbanne, France. (email: jerome.antoni@insa-lyon.fr)

Alessandro Paolo Daga is with the Dipartimento di Ingegneria Meccanica e Aerospaziale, Politecnico di Torino, Corso Duca degli Abruzzi 24, Torino, Italy. (email: alessandro.daga@polito.it)

Hongkun Li is with the School of Mechanical Engineering, Dalian University of Technology, 116024, China. (email: lihk@dlut.edu.cn)

Ning Chu is with the Institute of Process Equipment, College of Energy Engineering, Zhejiang University, Hangzhou 310027, China. (email: chuning@zju.edu.cn)

Siliang Lu is with the College of Electrical Engineering and Automation, Anhui University, Hefei 230601, China. (email: lusliang@mail.ustc.edu.cn)

Zhixiong Li is with Yonsei Frontier Lab, Yonsei University, Seoul 03722, Republic of Korea. (email: zhixiong.li@yonsei.ac.kr)

1. Introduction

Large-scale centrifugal compressors have been widely applied in the field of petrochemical, electrical, energy and aerospace industry [1]. However, with the growth of industrialization, centrifugal compressors are developing towards higher pressure ratios, higher speeds and larger flow rates making the working conditions of the impeller more and more severe and harsh [2]. Suffering the coupled variable aerodynamic load, the centrifugal force, the friction force etc., the blades are prone to high cycle fatigue, which will lead to the occurrence of fatigue failure under the long-term effect of alternating stresses [3-5]. Therefore, it is urgently needed to develop effective condition monitoring and vibration measurement techniques for the high-speed impeller to ensure its long-term reliable operation. Traditionally, strain tests are used to determine the vibration characteristic and changing trend of the rotating blades [6,7]. However, as it belongs to the branch of contact measurement methods, the installation of strain gauges and their wiring, is the key factor for a successful experiment, but it is a very complex and difficult procedure. In addition, it is unrealistic to stick strain gauges on all blades because the arrangement would be too complex, so the vibration of all the blades will not be measured simultaneously. Furthermore, safety problems may arise as the large centrifugal forces induced by high rotational speeds could throw the gauges away creating a potentially dangerous environment. On the contrary, the non-contact measurement technique called blade tip timing (BTT) is able to recover the vibration amplitude of all the blades simultaneously by acquiring the time at which each blade passes in front of the tip-timing sensors mounted on the casing, without causing safety issues. That is why it has attracted considerable attention and research effort in past decades [8-10].

Some valuable research works for blade vibration characteristics identification based on BTT technique have been conducted by scholars. For example, S. Heath improved the speed-vector-end-tracking technique to estimate the vibration amplitude of the blade during a linear frequency sweep excitation from the displacement vs. rotational speed plot. As just one BTT sensor is used in this technique, it is also called the “single-parameter method”. However, it is not able to estimate accurately the resonance frequency of the vibrating blade and only the rotational speed can be obtained. Considering that the synchronous resonance frequency is the product of the rotational frequency and the engine-order, the Campbell diagram is thus essential for the assessment of the resonance [11]. In order to overcome this shortcoming, S. Heath further proposed a two-parameter method based on two mounted BTT sensors, using a linear frequency sweep to identify both the synchronous resonance frequency and the amplitude of the vibrating blade, which was also verified by experiments [12]. Carrington focused on global autoregressive (GAR) methods to estimate the blade synchronous resonance parameters through equally spaced sensors. Differently from the empirical approach proposed by S. Heath, the GAR method identifies a parametric model of the blade vibration at constant impeller speed [13]. In order to improve the identification of synchronous vibrations, Wang et al. introduced a sweep frequency fitting technique which shows advantages over the GAR methods when less than four BTT sensors are used. The effectiveness of the proposed technique was verified both by simulation analysis and experimental study [14]. In some practical cases, the key-phase (once-per revolution) sensor is rather difficult to install which may limit the application of BTT. For solving this issue, Guo et al. put forward a tip-timing technique without once-per revolution sensor to identify the blade resonance parameters by utilizing the cross-correlation between the blades installation errors and the sequence derived from the tip-timing signal. Experiments were further designed and

conducted to verify the effectiveness of this technique [15]. In order to face the problem of an insufficient BTT sampling frequency compared to the blade vibration, some scholars studied several effective signal reconstruction algorithms for extracting original frequencies from the under-sampled signal and applied the algorithms both on simulated and experimental data [16-20]. Most of the aforementioned research works are focused on aero-engines with straight blades, while references in the literature about BTT condition monitoring and identification of centrifugal compressors (especially large-scale) remain rare. Obviously centrifugal compressors are substantially different from aero-engines in terms of size, flow field and impeller geometry, although they share a similar structural architecture, so that an analysis of the BTT technique applied on such machines is of great importance for the development of condition monitoring systems and for the improvement of maintenance programs. It is one goal of this paper to bridge this gap.

Another goal is to improve the robustness of BTT with respect to some sources of uncertainty and errors. It should be stressed that high accuracy of the time measurements is necessary in BTT to ensure reliable estimation of the blade vibration amplitudes, as the linear velocity of the blade tip is usually very large. However, as mentioned by P. Russhard and G. Rossi, some uncertainty will always remain [21-22]. The blades will never be perfectly equispaced for example, so that a calibration phase will be needed for compensating such angular imperfections. The time resolution will always be limited by the maximum frequency of the acquisition card. Furthermore, the casing will slightly vibrate during the high-speed rotation of the impeller, resulting in a shift of the tip-timing sensors and of the key-phase sensor, so that the blades arrival times will be affected by further error. Therefore, it is important to quantitatively analyze the effect of these factors on the resulting blade vibration amplitude and propose a way to alleviate them. Additional error could also come from the fact that the speed of the compressor may not be perfectly constant during a revolution, but this will not be analyzed in this work. As far as the authors know, few references have addressed the aforementioned issues. Hu estimated the signal reconstruction error affected by the parameters of the selected interpolating function qualitatively [17]. Satish considered several probable sources of errors in the measurement process from both the engine and BTT test system [23]. But the corresponding strategies on how to reduce errors were not presented in these works. Therefore, Pan analyzed several measurement uncertainties in BTT data and proposed a Basis Pursuit De-noising (BPDN) technique for alleviating these uncertainties in the spectrum recovery process for a blade multi-mode vibration [19]. He also performed simulations and experiments to prove the feasibility of the proposed technique. Nevertheless, this technique only focused on the accurate identification of frequencies while the vibration amplitudes corresponding to the recovered frequencies may be still inaccurate. However, it is of great importance to guarantee the accuracy and reliability also for the blade vibration amplitudes, which can be used for further analysis, to obtain for example the damping ratio or other vibration parameters of interest. An improved improve BTT method without once per revolution reference is proposed by Chen and verified on a small turbo fan. Nevertheless, despite an error reduction is experimentally shown, no theoretical basis is built to systematically study the error propagation from the sources to the BTT results [24].

In order to apply BTT technique for the vibration monitoring of centrifugal compressor blades and ensure the reliability of the measurement, the effect of the experimental errors on the measurement results is theoretically analyzed in detail and an improved BTT technique is

proposed on the basis of such results. Differently from the traditional BTT, the key-phase signal is not used here as the time-zero reference point but only as a mean to group the tip-timing signal to guarantee the correspondence to each physical blade. The time-zero reference point will be obtained by processing the tip-timing signal. Experiments on a centrifugal compressor test-rig verify the effectiveness of the improved technique. In addition, the resolution error and the corresponding optimization scheme are also carefully studied.

This paper is organized as follows: section 2 introduces the theoretical principles of BTT vibration measurements, the specific practical analysis and the calculation procedure. In section 3, the resolution error and sensors vibration error with estimated speed considerations are analyzed in detail, so as to understand the error propagation and counteract it. Next, some considerations regarding the geometrical error compensation are also given. Then, an improved technique is proposed in section 4 to sharpen the BTT accuracy and reliability. The application of the improved BTT technique on a large centrifugal compressor test-rig with a cracked blade is presented in section 5. In section 6, a dynamic model is built and its results are analyzed to explain the obtained experimental behavior. Finally, conclusions are given in section 7.

2 The description of the BTT technique

2.1 Principles of BTT vibration measurement

The most used sensors in BTT technique include fiber optic sensors, electric eddy current sensors etc., which can be used to trigger a clock. Tip-timing signal usually comes from fiber optic sensors mounted on the casing and called tip-timing sensors, while the key-phase sensor (often named as once-per revolution sensor), also mounted on the casing, will be placed near the rotating shaft, as depicted in Fig. 1. The principle of BTT is based on sampling the time at which a blade passes in front of a tip-timing sensor to produce time series.

Specifically, the procedure starts with a calibration phase, in which non-vibrating blades are monitored by acquiring their arrival time series $\left\{t_i^{idl}\right\}$ synchronously with the key-phase signal. Then a second acquisition is performed in the working condition, when the blades are in their vibrational state, to obtain the arrival time series $\left\{t_i\right\}$. In the end, the vibration amplitude of each blade can be calculated based on the difference of the time series between the calibration and the working condition. Differently from the traditional strain technique, BTT can simultaneously measure all the blade vibration amplitudes at the same time with the advantage of being a non-contact measurement (no gauges and wiring on the impeller). However, this produces the need of unique identification of the blades and the sensors. Specifically, suppose there are N sensors mounted on the casing along the circumferential direction and there exist M blades in the impeller. Taking the key-phase sensor angular position as a reference, index j is used to name the sensors as $0,1,...,N-1$ starting from the one closest to the key-phase (TT_0 in Fig. 1) in the direction opposite to the impeller rotation and continue in such direction. The angle $\alpha_j (0 \le j < N)$ characteristic of each sensor will be defined according to this criterion, starting from the key-phase angular position in the direction opposite to the rotation (The rotation is clockwise in

This article has been accepted for publication in a future issue of this journal, but has not been fully edited. Content may change prior to final publication. Citation information: DOI 10.1109/TIM.2020.3033463, IEEE Transactions on Instrumentation and Measurement

Fig.1). In the same way, index i will be used to label the blades as $0,1,...,M-1$ starting from closest to the key-phase in the direction opposite to the impeller rotation (blade 0) and going on in the same direction. The angle $\theta_i (0 \le j < M)$ which defines each blade will be measured from the key-phase angular position in the direction opposite to rotation. For ideal, equally spaced blades, one has $\theta_i = \theta_0 + 2\pi i / M$. Based on these definitions, the time at which the blade i passes through sensor j at the n-th cycle in ideal conditions (no blades vibration, constant rotational speed f) can be calculated by the following Eq. (1):

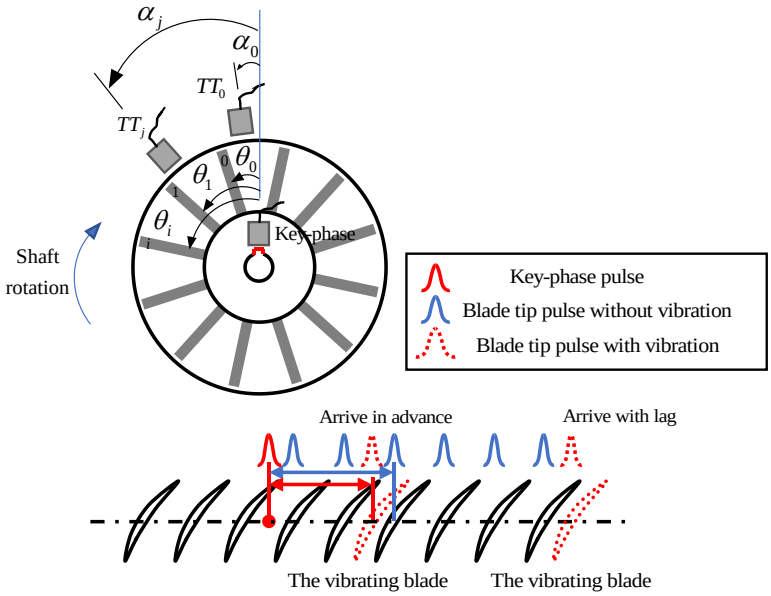

Fig. 1. Schematic diagram for vibration measurement principle of the BTT technique.

$$t_{i,n}^{j,idl} = \frac{1}{2\pi f}(\theta_i - \alpha_j + 2\pi n) . \tag{1}$$

However, when the vibrational state is considered, an error will arise, as the real blade angle will differ from the theoretical one, as shown in Fig. 1. The formula can then be corrected to account for the angular difference $\beta(t_{i,n}^j)$, as reported in Eq. (2),

$$t_{i,n}^j = \frac{1}{2\pi f}(\theta_i - \alpha_j + 2\pi n - \beta(t_{i,n}^j)) . \tag{2}$$

Obviously, the arrival times at which the blade passes in front of the tip-timing sensor are different in normal and vibrational states. Accordingly, the blade vibration amplitudes can be calculated through the product of linear velocity of the blade tip and the difference between the ideal and real arrival times. Therefore, combining Eq. (1) with Eq. (2), the blade vibration amplitudes can be calculated by the following equation

$$s(t_{i,n}^j) = 2\pi f R(t_{i,n}^{j,idl} - t_{i,n}^j) = 2\pi f R \Delta t_{i,n}^j , \tag{3}$$

wherein R is the impeller radius. Eq. (3) shows the principle for measuring the blade vibration amplitudes through BTT technique.

This article has been accepted for publication in a future issue of this journal, but has not been fully edited. Content may change prior to final publication. Citation information: DOI 10.1109/TIM.2020.3033463, IEEE Transactions on Instrumentation and Measurement

The following section will introduce in detail the description on how to establish the correspondence between time series and physical blades, how to calculate the calibration value of each blade in the normal state and how to calculate the blade vibration amplitude in its vibrational state.

2.2 Practical analysis of the BTT technique

Before the start of the experiment, tip-timing sensors should be installed on the casing to acquire the time series at which the blades pass through the sensors and a key-phase sensor should be installed near the shaft of the compressor to obtain the speed synchronization signal. From the point of view of improving the test accuracy, in this work also the key-phase signal will be acquired from a fiber optic sensor, as for the tip-timing.

The key-phase signal has two functions in BTT technique: the first is to group the time series so as to easily map each time to its physical blade; the second function is to work as the time-zero reference for the calculation of blade vibration amplitudes as explained hereafter.

The blade closest to key-phase sensor is labeled as 0, and the others are labeled as $1,2,...M-1$ respectively, opposite to the rotational direction of the impeller. One key-phase signal and M tip-timing signals will be sampled when the impeller completes one revolution.

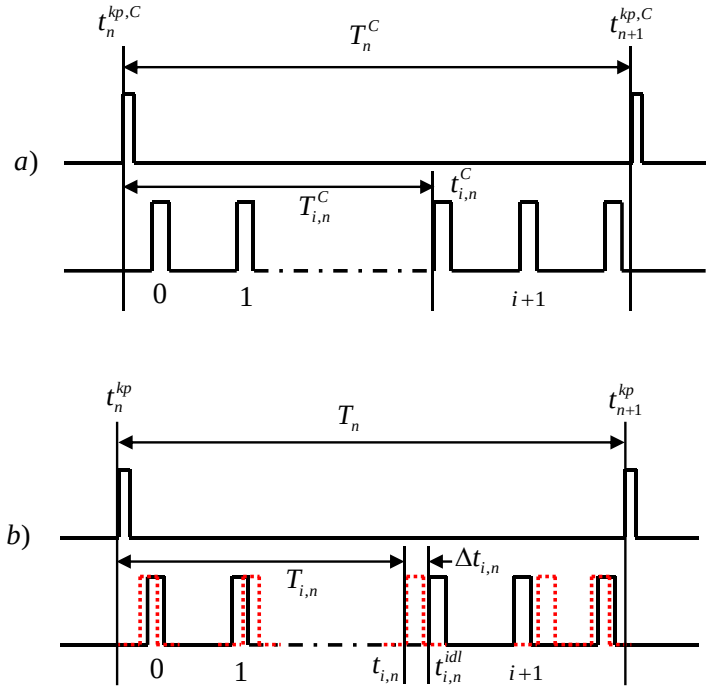

Fig. 2. Arrival times in the key-phase and tip-timing signals. (a) Measurements in the calibration process: $t_n^{kp,C}$ is the former key-phase arrival time in the n-th entire shaft revolution, $t_{n+1}^{kp,C}$ is the latter one and T_n^C is the rotation period. $t_{i,n}^C$ is the i-th blade arrival time in the n-th revolution and $T_{i,n}^C$ is the relative passage time. (b) Measurement for the vibrating blade: t_n^{kp}, t_{n+1}^{kp}, T_n and $T_{i,n}$ have similar definitions with those in the calibration process, and $\Delta t_{i,n}$ is the time difference due to the blade vibration.

As shown in Fig. 2(a), the n-th period T_n^C of the key-phase signal indicates that the

impeller has rotated one revolution (2π angle). Using the key-phase signal as time-zero reference, the i-th tip-timing passage time $T_{i,n}^{C}$ can be computed in calibration. Under the assumption of constant rotational speed during the revolution, the proportion $\gamma_{0i} / 2\pi = T_{i,n}^{C} / T_{n}^{C}$ can then be used to obtain the angle γ_{0i} that blade i has rotated relatively to key-phase sensor when it arrives at the tip-timing sensor. Given that the tip-timing sensor is fixed on the casing without any chance of movement (which also means that, from the theoretical point of view, the relative position between the tip-timing sensor and the key-phase sensor is fixed), as long as the assumption of constant speed during the revolution holds, the relative angle calculated through the above formula is a constant for every rotational speed, although the relative times $T_{i,n}^{C}$ will vary (the higher the rotational speed, the shorter the relative time which is the time difference between the i-th blade arrival time and the key-phase arrival time).

Based on this invariability, the constants $C_i = T_{i,n}^{C} / T_{n}^{C}$ can be computed in the calibration phase and will then be used to compute the ideal arrival time $t_{i,n}^{idl}$ of any blade i for all possible working conditions. It should also be noted that the values $C_0,...,C_{M-1}$ increase progressively with the index i, and being relative angles, they will be bounded in the range $0 < C_i < 1$ for $i = 0,1,...,M-1$. The actual arrival times will be compared (by subtraction) to such ideal times so that it will be possible to determine whether a blade is arrived in advance or with delay, as shown in Fig. 1. The vibration amplitude $s_{i,n}$ of any blade i can then be calculated by the following equation:

$$s_{i,n} = v * (T_{i,n} - C_i T_n) \tag{4}$$

where, v is the linear speed of the blade tip ($v = 2\pi fR$), T_n represents the period of key-phase signal measured in the actual experiment under different rotational speeds, C_i is the calibration constant previously introduced and $T_{i,n}$ is the time difference of i-th blade relative to the key-phase signal obtained when the blade is vibrating.

3 Error analysis of the traditional BTT technique

A factor which strongly affects the BTT performance is the accuracy of the measurement. The main issue related to centrifugal compressors blades is that the vibration amplitude will be in general quite limited because of the large stiffness, so high amplitude resolution is needed to guarantee precision and accuracy. Therefore, it is of great significance to conduct a theoretical analysis on the errors affecting the measurement, so as to highlight the bottlenecks and propose

This article has been accepted for publication in a future issue of this journal, but has not been fully edited. Content may change prior to final publication. Citation information: DOI 10.1109/TIM.2020.3033463, IEEE Transactions on Instrumentation and Measurement

improvements accordingly. In this paper, the main sources of errors will be considered; in particular, the time resolution error of the digital acquisition system will be discussed together with the further random error induced by experimental uncertainties. All these sources of random errors in fact produce the same effect of introducing a deviation in the measured arrival times of both the key-phase and tip-timing signals.

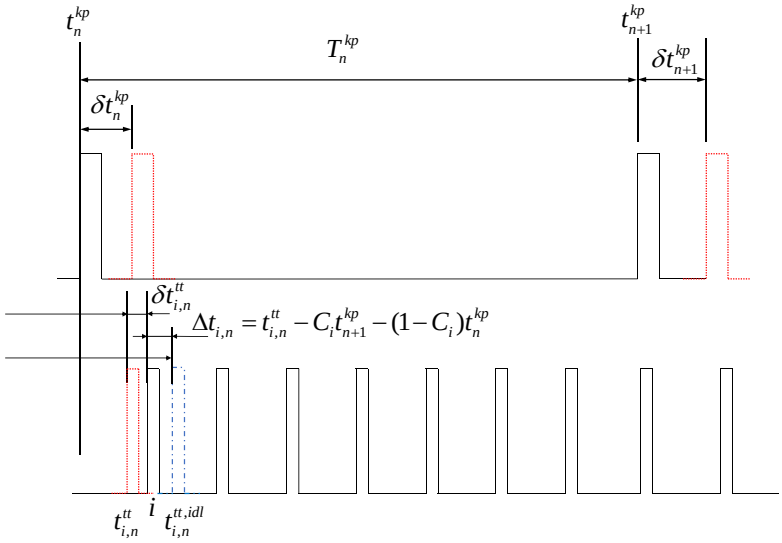

Fig. 3. Arrival time errors in the key-phase and tip-timing signals induced by experimental uncertainties: δt_n^{kp} is the arrival time error of the former key-phase signal in the n-th entire shaft revolution and δt_{n+1}^{kp} is the latter one. $\delta t_{i,n}^{tt}$ is the i-th blade arrival time error and $\Delta t_{i,n}$ is the time difference between the ideal arrival time and the actual one induced by the blade vibration without measurement error.

According to the notation used in this paper, focusing on the n-th entire shaft revolution, the former key-phase arrival time is defined as t_n^{kp} and the latter one is defined as t_{n+1}^{kp}. Then the period will be referred to as $T_n^{kp} = t_{n+1}^{kp} - t_n^{kp}$, while the i-th blade tip-timing measure will be called $t_{i,n}^{tt}$. The same notation is kept in calibration to compute the constant $C_i = \left[\dfrac{t_{i,n}^{tt} - t_n^{kp}}{t_{n+1}^{kp} - t_n^{kp}} \right]_C$ at constant low-speed and stationary operational condition. Then, the time difference between the ideal and the actual blade arrivals is expressed as

$$\begin{aligned} \Delta t_{i,n} &= t_{i,n}^{tt} - t_{i,n}^{tt,idl} = t_{i,n}^{tt} - \left[t_n^{kp} + \left(\frac{t_{i,n}^{tt} - t_n^{kp}}{T_n^{kp}} \right)_C T_n^{kp} \right] = \\ &= t_{i,n}^{tt} - t_n^{kp} - C_i T_n^{kp} = t_{i,n}^{tt} - t_n^{kp} - C_i \left(t_{n+1}^{kp} - t_n^{kp} \right) = \\ &= t_{i,n}^{tt} - C_i t_{n+1}^{kp} - (1 - C_i) t_n^{kp} \end{aligned} \quad , \tag{5}$$

where C_i is used to map the calibration tip time to its theoretical value, compensating for the

speed difference among the calibration and the actual working condition.

Based on the above definitions, assuming a given rotational speed f, one can study the error propagation on the vibration amplitude focusing on the time difference (Eq. (3)). A sensitivity analysis on the $\Delta t_{i,n}$ can then be performed starting from the partial derivatives,

$$\frac{\partial \Delta t_{i,n}}{\partial t_{i,n}^{tt}} = 1, \qquad \frac{\partial \Delta t_{i,n}}{\partial t_{n+1}^{kp}} = -C_i, \qquad \frac{\partial \Delta t_{i,n}}{\partial t_{n}^{kp}} = -(1 - C_i). \tag{6}$$

The error affecting such time difference turns out to be bounded by

$$\delta \Delta t_{i,n} = \left| \frac{\partial \Delta t_{i,n}}{\partial t_{i,n}^{tt}} \right| \delta t_{i,n}^{tt} + \left| \frac{\partial \Delta t_{i,n}}{\partial t_{n+1}^{kp}} \right| \delta t_{n+1}^{kp} + \left| \frac{\partial \Delta t_{i,n}}{\partial t_{n}^{kp}} \right| \delta t_{n}^{kp}. \tag{7}$$

However, this estimate is often found too large to be of practical interest. Assuming mutual independence of the errors, the average squared error can be expressed as the sum of the squared contributions from the tip-timing and from the key phase measurements; as follows,

$$\left(\delta \Delta t_{i,n}\right)^2 = \left(\frac{\partial \Delta t_{i,n}}{\partial t_{i,n}^{tt}} \delta t_{i,n}^{tt} \right)^2 + \left(\frac{\partial \Delta t_{i,n}}{\partial t_{n+1}^{kp}} \delta t_{n+1}^{kp} \right)^2 + \left(\frac{\partial \Delta t_{i,n}}{\partial t_{n}^{kp}} \delta t_{n}^{kp} \right)^2$$

$$\left|\delta \Delta t_{i,n}\right| = \sqrt{\left(\delta t_{i,n}^{tt}\right)^2 + \left(C_i \delta t_{n+1}^{kp}\right)^2 + \left((1 - C_i)\delta t_{n}^{kp}\right)^2}. \tag{8}$$

This error will further be magnified in the amplitude vibration (Eq. (9)):

$$\delta s = 2\pi f R \cdot \delta \Delta t_{i,n}, \tag{9}$$

where constant speed f is assumed.

Relevant observations can be obtained considering alternatively the different sources of random errors.

3.1 The resolution error

The resolution error is caused by the finite sampling rate of data acquisition equipment in the monitoring system and is unavoidable. Specifically, the continuous vibration signal of the blade cannot be acquired in the actual measurement process and just discrete data points can be sampled through the data acquisition card (e.g. National Instruments DAQ etc.) with a finite sampling rate, which will lead to the existence of a deviation between the measured blade arrival time and the actual blade arrival time and the error will propagate to the computed blade vibration amplitude. The magnitude of the resolution error is mainly influenced by the internal time base of the acquisition card and Fig. 4 is used here to explain how the finite internal time base affects the measurement result of the blade arrival time.

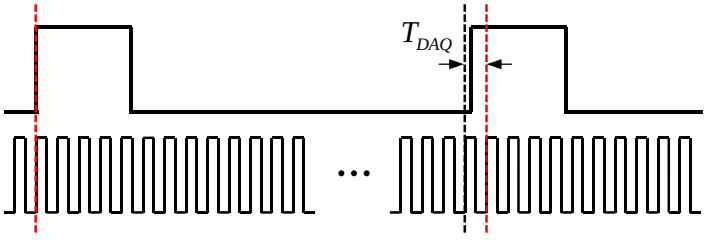

Fig. 4. Analysis of the resolution error, where T_{DAQ} is the maximum arrival time error both for key-phase and tip-timing signal induced by the data acquisition card.

More precisely, suppose that the period of internal time base of the acquisition card is $T_{DAQ}=1/f_{DAQ}$, then, if the n-th time base pulse has already passed when the sensor triggers the acquisition card, the sample will correspond to the $n+1$-th time base, resulting in a maximum error of $\delta t^r = T_{DAQ}$ both for tip-timing and key-phase signals.

The timing error will propagate to a vibration amplitude error δs^r, which can be found by mapping the δt^r through Eq. (9). The resulting expression, Eq. (10), follows:

$$\begin{aligned}\delta s^r &= 2\pi fR\cdot\sqrt{\left(\delta t^r\right)^2+\left(C_i\delta t^r\right)^2+\left((1-C_i)\delta t^r\right)^2}\\ &= 2\pi fR\cdot\delta t^r\sqrt{\left(2C_i^2-2C_i+2\right)}=\delta t^r\cdot 2\sqrt{2}\pi fR\sqrt{\left(C_i^2-C_i+1\right)}\end{aligned} \tag{10}$$

where, f is the rotational frequency of the impeller and R is the impeller radius.

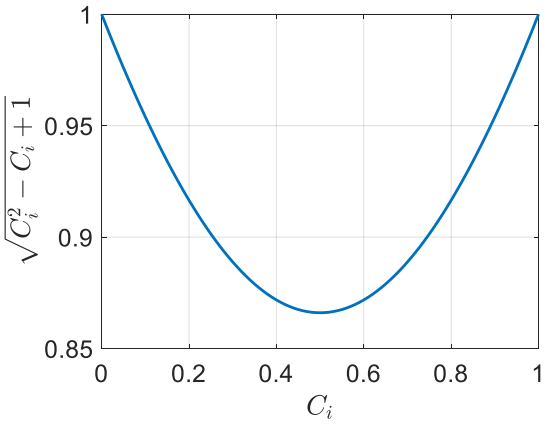

Fig. 5. The trend of blade related term $\sqrt{C_i^2-C_i+1}$ with the calibration value C_i.

It can be found from Eq. (10) that the blade index i will affect the error decreasing it for mid i blades, as shown in Fig. 5. As the effect of the blade related term $\sqrt{\left(C_i^2-C_i+1\right)}$ is always smaller than 1, one could neglect it considering the conservative relation:

$$\delta s^r \approx \delta t^r\cdot 2\sqrt{2}\pi fR. \tag{11}$$

Focusing on this formula, the amplitude error induced by the resolution will increase by incrementing the rotational frequency or the impeller radius, so it is not even constant during the working conditions. As the impeller structure and rotational speed range of the compressor have already been determined at the design stage to meet the industrial needs, it is unrealistic to reduce the vibration amplitude error by narrowing the impeller radius and the speed range, so the only

possible optimization is on the acquisition board. For explaining this issue in detail, the compressor under analysis in this work is used. Suppose the required amplitude resolution for the vibrational blade is 0.01 mm, the impeller diameter is 800 mm and the blade maximum rotational speed is 6000 rpm, then the required timing error for the system should be less than $\delta t_{MAX} = 0.01mm \Big/ \left(2\sqrt{2}\, fR\right) = 28\,\text{ns}$. Therefore, the high-speed clock rate in the acquisition card should be at least $1/\delta t_{MAX} = 36\,\text{MHz}$. Finally, an 80 MHz high-speed counter card is selected in our test to improve the resolution accuracy as much as possible, as other random errors will also affect the final vibration amplitude.

3.2 Vibration of the sensors

Relevant observations can be obtained considering the experimental error corresponding to the vibration of the sensors. Specifically, as the tip-timing and key-phase sensors are both installed on the same casing, one can imagine that they undergo a vibration of amplitude δp (Fig. 6).

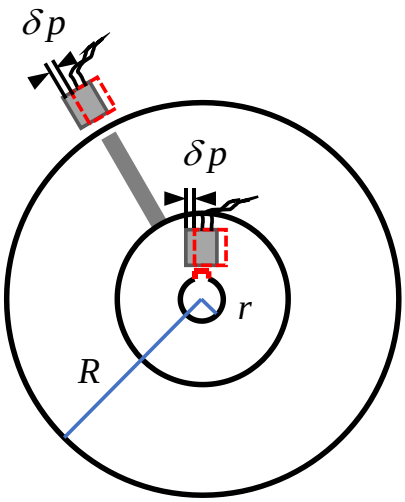

Fig. 6. Schematic diagram for the vibration of the sensors: δp is the vibration amplitude of sensors, r is the shaft radius and R is the impeller radius.

Since for large-scale centrifugal compressor the impeller radius R is much larger than the shaft radius r, the induced error in terms of angle will be much larger for the key-phase sensor, due to $\delta\alpha^{tt} = \delta p \big/ R < \delta p \big/ r = \delta\alpha^{kp}$, meaning that the key-phase arrival times will be affected in a more serious way with respect to the tip-timing arrival times. This can be taken into account by introducing the ratio reported in Eq. (12) and (13), which holds under the constant speed hypothesis:

$$\delta t^{tt} = \frac{\delta\alpha^{tt}}{2\pi f} = \frac{\delta p \big/ R}{2\pi f}, \tag{12}$$

$$\frac{\delta t^{tt}}{\delta t^{kp}} = \frac{\delta\alpha^{tt}}{\delta\alpha^{kp}} = \frac{\delta p \big/ R}{\delta p \big/ r} = \frac{r}{R}, \tag{13}$$

This article has been accepted for publication in a future issue of this journal, but has not been fully edited. Content may change prior to final publication. Citation information: DOI 10.1109/TIM.2020.3033463, IEEE Transactions on Instrumentation and Measurement

so that one can quantify the influence of the vibration error on the time difference error following the procedure proposed in Eq. (8). Finally, the induced vibration amplitude error can be obtained through Eq. (15).

$$\delta\Delta t = \sqrt{\left(\delta t^{tt}\right)^2 + \left(C_i \delta t^{kp}\right)^2 + \left((1-C_i)\delta t^{kp}\right)^2} = \sqrt{\left(\frac{r}{R}\delta t^{kp}\right)^2 + \left(2C_i^2 - 2C_i + 1\right)\left(\delta t^{kp}\right)^2} =$$

$$= \delta t^{kp}\sqrt{\left(2C_i^2 - 2C_i + \left(1+\left(\frac{r}{R}\right)^2\right)\right)} = \delta t^{tt}\frac{R}{r}\sqrt{\left(2C_i^2 - 2C_i + \left(1+\left(\frac{r}{R}\right)^2\right)\right)} \tag{14}$$

$$= \delta p \frac{1}{2\pi f r}\sqrt{\left(2C_i^2 - 2C_i + \left(1+\left(\frac{r}{R}\right)^2\right)\right)}$$

$$\delta s^v = \delta p \cdot \sqrt{2}\frac{R}{r}\sqrt{\left(C_i^2 - C_i + \frac{1}{2}\left(1+\left(\frac{r}{R}\right)^2\right)\right)} \cdot \tag{15}$$

This result is depicted in Fig. 7, where the relative error $\delta s^v/\delta p = \delta\Delta t/\delta t^{tt}$ is reported as a function of the calibration ratio C_i of each blade ($0 < C_i < 1$, $i = 0,1,...,M-1$) for some relevant geometric ratios R/r.

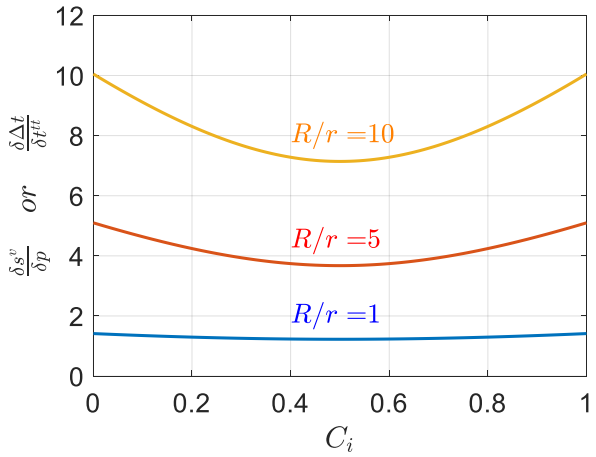

Fig. 7. The relative error $\delta s^v/\delta p = \delta\Delta t/\delta t^{tt}$ induced by sensors vibration as a function of the calibration value C_i.

Based on Fig. 7, one can find how the effect of the size can strongly magnify the measurement error, so that in many cases, the BTT result for large-scale centrifugal compressors ($R/r \gg 1$) will be corrupted by such influence. It should be also remembered that the values $C_0,...,C_{M-1}$ increase progressively with the index i, so it is possible to conclude that both the blades with low and high indices i will undergo more serious deviations with respect to the blades with medium i ($C_i \simeq 0.5$). In addition, for $R/r \gg 1$ then, one can use the

This article has been accepted for publication in a future issue of this journal, but has not been fully edited. Content may change prior to final publication. Citation information: DOI 10.1109/TIM.2020.3033463, IEEE Transactions on Instrumentation and Measurement

approximation:

$$\delta s^{v} \approx \delta p \cdot \sqrt{2} \frac{R}{r} \sqrt{\left(C_i^2 - C_i + \frac{1}{2} \right)} \tag{16}$$

for which, the blade related term is reported in Fig.8.

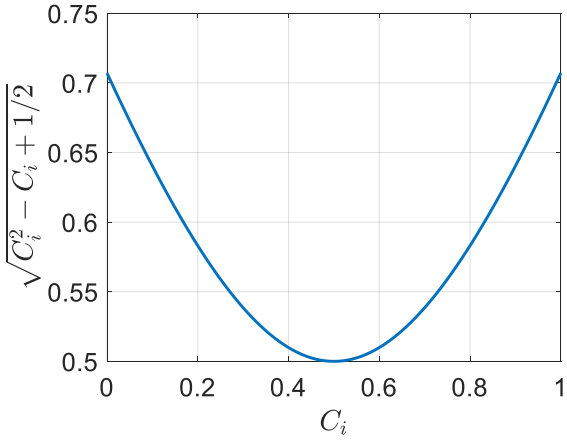

Fig.8. Trend of the blade related term $\sqrt{C_i^2 - C_i + 1/2}$ with respect to the calibration value C_i.

It can be seen from the graph, that the maximum of $1/\sqrt{2}$ is reached at the C_i extrema, so that it can be useful to further approximate to

$$\delta s^{v} \approx \delta p \cdot \sqrt{2} \frac{R}{r} \frac{1}{\sqrt{2}} = \delta p \cdot \frac{R}{r}. \tag{17}$$

It is also worth to note that, considering for example the case $R/r = 1$, Eq. (15) simplifies to $\delta s^{v} \approx \delta p \cdot \sqrt{2}$. The sensors vibration error magnification problem can be solved by acquiring the key-phase signal on a portion of shaft with larger diameter or by designing a stable bracket (isolated from vibration) far from the shaft, so that the final timing accuracy will be improved, but these are usually unhandy solutions and may introduce other errors, so an alternative improved technique is presented in this paper in chapter 4.

3.3 Geometrical errors

The previous subsections assumed exact knowledge of the values of the constants C_i, which correspond to the normalized angular positions of each blade $(\theta_i - \alpha)/2\pi$ relative to the sensor $j = 1$ ($\alpha_1 = \alpha$), as depicted in Fig. 1. This made it possible to account and compensate for possible manufacturing imperfections of the blades, which are never perfectly equispaced in reality. In practice, the true angular position of the blades with respect to the key phase sensor might also be subjected to uncertainties. The constants C_i will then be estimated in a stable, low

This article has been accepted for publication in a future issue of this journal, but has not been fully edited. Content may change prior to final publication. Citation information: DOI 10.1109/TIM.2020.3033463, IEEE Transactions on Instrumentation and Measurement

speed acquisition phase called calibration, and will usually be affected by an estimation error.

In the traditional BTT this estimate is computed relying on both the blade and the key-phase passage times. Assuming a constant rotational speed $f=\left(d\theta/2\pi\right)/dt$, angles and times are directly proportional, so that angular differences can be substituted by time differences. At each cycle n, an estimate $C_{i,n}$ can then be found, and these can be later averaged to improve the accuracy, as shown in Eq. (18)

$$\begin{aligned} C_{i,n} &= \left[\frac{t_{i,n}^{tt}-t_n^{kp}}{t_{n+1}^{kp}-t_n^{kp}}\right]_C \\ C_i &= \frac{1}{N}\sum_{n=1}^{N} C_{i,n} = \frac{1}{N}\sum_{n}\left[\frac{t_{i,n}^{tt}-t_n^{kp}}{t_{n+1}^{kp}-t_n^{kp}}\right]_C \end{aligned} . \tag{18}$$

The C_i estimate will then be affected by an error which propagates from the time measurements. This can be obtained following the same scheme based on the averaged squared error:

$$\delta C_i^2 = N\left(\left|\frac{\partial C_i}{\partial t_{i,n}^{tt}}\right|\delta t_C^{tt}\right)^2 + \left(N-1\right)\left(\left|\frac{\partial C_i}{\partial t_n^{kp}}\right|\delta t_C^{kp}\right)^2 + \left(\left|\frac{\partial C_i}{\partial t_1^{kp}}\right|\delta t_C^{kp}\right)^2 + \left(\left|\frac{\partial C_i}{\partial t_{N+1}^{kp}}\right|\delta t_C^{kp}\right)^2 . \tag{19}$$

The required partial derivatives are:

$$\begin{aligned} &\frac{\partial C_i}{\partial t_{i,n}^{tt}} = \frac{1}{N}\frac{1}{t_{n+1}^{kp}-t_n^{kp}} = \frac{1}{N}\frac{1}{T_n} \text{ for } n=1:N, \\ &\frac{\partial C_i}{\partial t_n^{kp}} = -\frac{1}{N}\frac{1}{T_n}(1-C_{i,n}) - \frac{1}{N}\frac{1}{T_{n-1}}C_{i,n-1} \text{ for } n=2:N, \\ &\frac{\partial C_i}{\partial t_1^{kp}} = -\frac{1}{N}\frac{1}{T_1}\left(1-C_{i,1}\right), \qquad \frac{\partial C_i}{\partial t_{N+1}^{kp}} = -\frac{1}{N}\frac{1}{T_N}C_{i,N} \end{aligned} \tag{20}$$

Being interested in the order of magnitude of the error, it is wise to use the hypothesis of stationarity during the calibration, which allows to drop the index n as, at every cycle, $T_n = T = 1/f$ and $C_{i,n} = C_i$.

Under this assumption,

$$\delta C_i = \frac{1}{\sqrt{N}}\frac{1}{T}\sqrt{\left(\delta t_C^{tt}\right)^2 + \frac{1}{N}\left(2C_i^2 - 2C_i + N\right)\left(\delta t_C^{kp}\right)^2} , \tag{21}$$

which can be further simplified assuming an equal amplitude for the time errors of the tip-times and of the key-phase times during the calibration phase

$$\delta C_i = \left[\frac{1}{T}\frac{1}{\sqrt{N}}\sqrt{\frac{1}{N}\left(2C_i^2 - 2C_i + 2N\right)}\right]\delta t_C . \tag{22}$$

This final formulation can be further simplified by considering that N can be arbitrarily large in the calibration procedure, so that $N \gg 1$. Remembering that the blade related term $C_i^2 - C_i + 1$ is limited in the range $\left(3/4\ 1\right)$ given $0 < C_i < 1$, then $0 \le C_i^2 - C_i \le 1/4$ is

negligible with respect to N. Under these assumptions, it comes

$$\delta C_i \le f \frac{1}{\sqrt{N}} \sqrt{2} \delta t_C . \tag{23}$$

It is relevant to remember that the calibration phase is independent of the measurement phase, so that the δC_i contribution can be easily summed up the other sources of errors.

3.4 Estimated speed errors considerations

Up to this point it has been assumed that the knowledge of the speed is given, but in some working conditions the rotation speed may be unknown and key-phase signal is used to estimate it. Then Eq. (3) should be modified to

$$\begin{aligned} s_{i,n}(t_{i,n}) &= \frac{2\pi R}{T_n} \Delta t_{i,n} = \\ &= 2\pi R \left[\frac{t_{i,n}^{tt} - t_n^{kp}}{t_{n+1}^{kp} - t_n^{kp}} - \left(\frac{t_{i,n}^{tt} - t_n^{kp}}{t_{n+1}^{kp} - t_n^{kp}} \right)_C \right] = 2\pi R \left[K_i - C_i \right] \end{aligned} \tag{24}$$

where K_i, is the angle of the i-th blade relative to key-phase position under the vibration state of the blade. The difference between K_i and C_i is that C_i is obtained under the non-vibration state of the blade (the calibration stage).

Performing a sensitivity analysis on this formula one can get

$$\frac{\partial s_{i,n}}{\partial t_{i,n}^{tt}} = \frac{2\pi R}{T_n}, \quad \frac{\partial s_{i,n}}{\partial t_{n+1}^{kp}} = -K_i \frac{2\pi R}{T_n}, \quad \frac{\partial s_{i,n}}{\partial t_n^{kp}} = -(1-K_i) \frac{2\pi R}{T_n}, \quad \frac{\partial s_{i,n}}{\partial C_i} = -2\pi R, \tag{25}$$

$$\delta s^2 = \left(\frac{2\pi R}{T_n} \right)^2 \left[\left(\delta t^{tt} \right)^2 + \left(K_i \delta t^{kp} \right)^2 + \left((1-K_i) \delta t^{kp} \right)^2 + \left(\frac{\sqrt{2}}{\sqrt{N}} \cdot \delta t_C \right)^2 \right], \tag{26}$$

from which the different sources of errors can be analyzed. For simplicity, in this analysis N is assumed to be big enough so that the term related to the geometric error will be considered negligible with respect to the other contributions.

Considering the resolution error one can get

$$\delta s^r = \delta t^r \cdot \frac{2\pi R}{T_n} \sqrt{2K_i^2 - 2K_i + 2} , \tag{27}$$

where the term $\sqrt{K_i^2 - K_i + 1}$ changes from previous computation but has actually the same trend and the same maximum of 1 in the range $0 < K_i < 1$ of interest, so that the resolution error can still be considered well approximated by

$$\delta s^r \approx \delta t^r \cdot 2\sqrt{2} \pi f R . \tag{28}$$

Similarly, assuming unknown but constant speed, the formula for the error related to sensors vibration becomes

This article has been accepted for publication in a future issue of this journal, but has not been fully edited. Content may change prior to final publication. Citation information: DOI 10.1109/TIM.2020.3033463, IEEE Transactions on Instrumentation and Measurement

$$\delta s^{v} = \delta t^{kp} \sqrt{\left(K_i^2 - K_i + \frac{1}{2}\left(1 + \left(\frac{r}{R} \right)^2 \right) \right)} \ , \tag{29}$$

$$\delta s^{v} = \delta p \cdot \sqrt{2} \frac{R}{r} \sqrt{\left(K_i^2 - K_i + \frac{1}{2}\left(1 + \left(\frac{r}{R} \right)^2 \right) \right)} \ , \tag{30}$$

which, for the particular case $R/r = 1$, simplifies to:

$$\delta s^{v} \approx \delta p \cdot \sqrt{2} \ . \tag{31}$$

4 The improved BTT technique

Based on the deep analysis above, it can be clearly found that the accuracy of BTT technique is seriously affected by the deviation of the key-phase signal induced by the casing vibration. In order to remove the strong effect of the size (R/r) while improving the accuracy and the precision of the measurement, an improved technique is here proposed, able to enhance the BTT diagnostic ability with a specific focus on large-scale centrifugal compressor blades.

In particular, the idea is to use the key-phase signal only to match the physical blades with the sampled tip-timing signals, grouping the blades that pass the tip-timing sensor in one revolution. The key phase measures t_n^{kp} and t_{n+1}^{kp} will then be substituted with more accurate estimates obtained from the tip-timing sensors $\hat{t}_n^{kp}$ and $\hat{t}_{n+1}^{kp}$, as shown in Fig. 9.

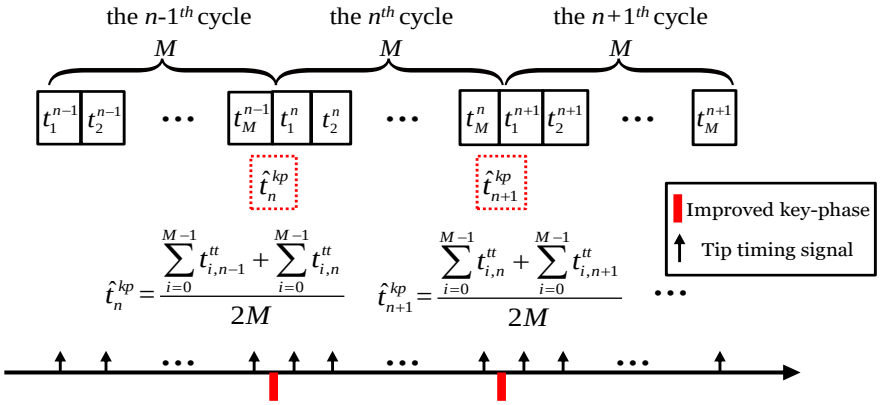

Fig. 9. Principle of the improved algorithm.

These values will be determined as the expected values of the tip-timing signals in the $n-1$ -th, n-th and $n+1$-th groups (revolutions), as shown in Eq. (32).

$$\hat{t}_n^{kp} = \frac{\sum_{i=0}^{M-1} t_{i,n-1}^{tt} + \sum_{i=0}^{M-1} t_{i,n}^{tt}}{2M}, \qquad \hat{t}_{n+1}^{kp} = \frac{\sum_{i=0}^{M-1} t_{i,n}^{tt} + \sum_{i=0}^{M-1} t_{i,n+1}^{tt}}{2M}. \tag{32}$$

Then, the calibration will be acquired based on the above estimates, as shown in Eq. (33). It is worth to underline that, to improve estimation of the calibration coefficients C_i, an average on N cycles is also recommended

This article has been accepted for publication in a future issue of this journal, but has not been fully edited. Content may change prior to final publication. Citation information: DOI 10.1109/TIM.2020.3033463, IEEE Transactions on Instrumentation and Measurement

$$C_i = \frac{1}{N-2}\sum_{n=2}^{N-1} C_{i,n} = \frac{1}{N-2}\sum_{n=2}^{N-1} \frac{t_{i,n}^{tt} - \hat{t}_n^{kp}}{\hat{t}_{n+1}^{kp} - \hat{t}_n^{kp}}\Bigg|_C , \tag{33}$$

Finally, the estimated period $\hat{T}_n = \hat{t}_{n+1}^{kp} - \hat{t}_n^{kp}$ is used in this paper to compute the actual mean rotation frequency during the revolution. Eq. (34) summarizes then the BTT vibration amplitude result for the proposed technique

$$s_{i,n} = \frac{2\pi R}{\hat{T}_n}\left(t_{i,n}^{tt} - \hat{t}_n^{kp} - C_i\hat{T}_n\right). \tag{34}$$

It can be found that the key-phase signal is not involved in the specific Eq. (34), and its function is just to guarantee the correspondence between the tip-timing signals and the physical blades. Therefore, the measurement error induced by casing vibration can be effectively reduced, and the proposed technique can be thought as an improved BTT algorithm without the key-phase signal.

In order to verify the superiority of the improved algorithm, the error propagation scheme can be compared to the one of usual BTT of Fig. 7, assuming a given speed f :

$$s_i = 2\pi fR\Delta t_{i,n} = 2\pi fR\left(t_{i,n}^{tt} - \hat{t}_n^{kp} - C_i\hat{t}_{n+1}^{kp} + C_i\hat{t}_n^{kp}\right), \tag{35}$$

$$\Delta t_{i,n} = t_{i,n}^{tt} - \frac{1}{2M}\left(\sum_{i=0}^{M-1} t_{i,n-1}^{tt} + \sum_{i=0}^{M-1} t_{i,n}^{tt}\right) - \frac{C_i}{2M}\left(\sum_{i=0}^{M-1} t_{i,n}^{tt} + \sum_{i=0}^{M-1} t_{i,n+1}^{tt}\right) + \frac{C_i}{2M}\left(\sum_{i=0}^{M-1} t_{i,n-1}^{tt} + \sum_{i=0}^{M-1} t_{i,n}^{tt}\right), \tag{36}$$

the error propagation can then be studied via partial derivatives, leading to

$$\frac{\partial \Delta t_{i,n}}{\partial t_{i,n}^{tt}} = 1 - \frac{1}{2M},\ \left.\frac{\partial \Delta t_{i,n}}{\partial t_{k,n}^{tt}}\right|_{k\neq i} = -\frac{1}{2M},\ \frac{\partial \Delta t_{i,n}}{\partial t_{i,n+1}^{tt}} = -\frac{C_i}{2M},\ \frac{\partial \Delta t_{i,n}}{\partial t_{i,n-1}^{tt}} = -\frac{C_i - 1}{2M}, \tag{37}$$

$$\delta\Delta t_{i,n}^2 = \left(\delta t^{tt}\frac{\partial \Delta t_{i,n}}{\partial t_{i,n}^{tt}}\right)^2 + (M-1)\left(\delta t^{tt}\left.\frac{\partial \Delta t_{i,n}}{\partial t_{k,n}^{tt}}\right|_{k\neq i}\right)^2 + M\left(\delta t^{tt}\frac{\partial \Delta t_{i,n}}{\partial t_{i,n+1}^{tt}}\right)^2 + M\left(\delta t^{tt}\frac{\partial \Delta t_{i,n}}{\partial t_{i,n-1}^{tt}}\right)^2. \tag{38}$$

$$\delta\Delta t_{i,n} = \delta t^{tt}\sqrt{\frac{1}{2M}\left[C_i^2 - C_i + 2M - 1\right]} \tag{39}$$

Considering resolution error, one can obtain

$$\delta s^r = 2\pi fR\cdot\delta t^r\sqrt{\frac{1}{2M}\left[C_i^2 - C_i + 2M - 1\right]}. \tag{40}$$

And accounting for sensors vibration, it is easy to find

$$\delta s^v = 2\pi fR\cdot\delta t^{tt}\sqrt{\frac{1}{2M}\left[C_i^2 - C_i + 2M - 1\right]} = \delta p\sqrt{\frac{1}{2M}\left[C_i^2 - C_i + 2M - 1\right]}. \tag{41}$$

Fig. 10 helps to visualize the comparison of Eq. (15) with the optimal ratio $R/r = 1$ to Eq. (41) with some specific values of M . It is relevant to point out that the same graph holds also for comparing Eq. (40) to Eq. (10). As a matter of fact, it is easy to prove that $\left.\frac{\delta s^v}{\delta p}\right|_{R/r=1} = \frac{1}{2\pi fR}\frac{\delta s^r}{\delta t^r}$, for the traditional BTT and $\frac{\delta s^v}{\delta p} = \frac{1}{2\pi fR}\frac{\delta s^r}{\delta t^r}$ for the improved BTT for any M .

This article has been accepted for publication in a future issue of this journal, but has not been fully edited. Content may change prior to final publication. Citation information: DOI 10.1109/TIM.2020.3033463, IEEE Transactions on Instrumentation and Measurement

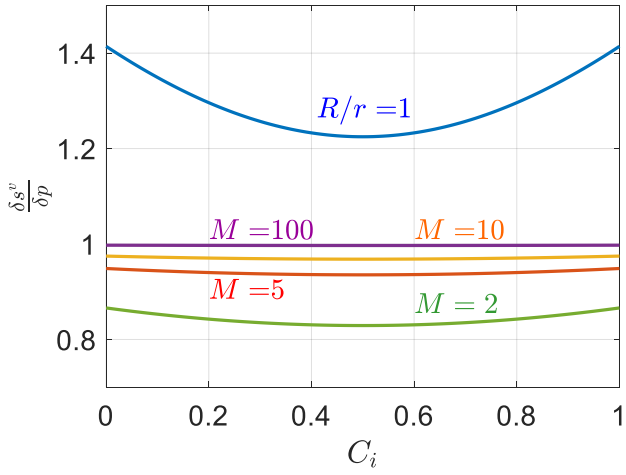

Fig. 10. Relative error $\delta s^v/\delta p$ induced by sensors vibration as a function of the calibration ratio for the optimal traditional BTT with $R/r=1$ and for the improved BTT with $M=2,5,10,100$ blades.

The improved BTT performance results are limited by the number of blades, but, in any case, the graph in Fig. 10 clearly shows that for any $M>1$ it is better than the traditional BTT even in the optimal case $R/r=1$ both with respect to sensors vibration and to resolution errors, this underlines the ability of the improved BTT to limit the error propagation and to compensate for differential effects on the different blades (the curves tends to become flat as M becomes larger).

Furthermore, it is interesting to note that since, C_i is limited in the range $(0\ 1)$, $3/4\le C_i^2-C_i+1\le 1$, therefore Eq. (41) reduces to

$$\delta s^v \approx \delta p\sqrt{\frac{2M-2}{2M}}=\delta p\sqrt{\frac{M-1}{M}}, \tag{42}$$

and Eq. (40) becomes

$$\delta s^r \approx 2\pi fR\cdot\delta t^r\sqrt{\frac{M-1}{M}}\to 2\pi fR\cdot\delta t^r. \tag{43}$$

These above results have been obtained for a given speed f, yet further considerations on the speed estimation also possible for the improved BTT technique.

Considering Eq. (34) one can write

$$\begin{aligned} s_{i,n}&=2\pi R\frac{\Delta t_{i,n}}{\hat{T}_n}=2\pi R\frac{\Delta t_{i,n}}{\hat{t}_{n+1}^{kp}-\hat{t}_n^{kp}}=2\pi R\left(\frac{t_{i,n}^{tt}-\hat{t}_n^{kp}-C_i\hat{t}_{n+1}^{kp}+C_i\hat{t}_n^{kp}}{\hat{t}_{n+1}^{kp}-\hat{t}_n^{kp}}\right)\\ &=2\pi R\left(\frac{t_{i,n}^{tt}-\hat{t}_n^{kp}}{\hat{t}_{n+1}^{kp}-\hat{t}_n^{kp}}-\frac{C_i\hat{t}_{n+1}^{kp}-C_i\hat{t}_n^{kp}}{\hat{t}_{n+1}^{kp}-\hat{t}_n^{kp}}\right)=2\pi R\left(K_i-C_i\right)\end{aligned}, \tag{44}$$

$$s_{i,n}=2\pi R\left(\frac{2Mt_{i,n}^{tt}-\left(\sum_{i=0}^{M-1}t_{i,n-1}^{tt}+\sum_{i=0}^{M-1}t_{i,n}^{tt}\right)}{\sum_{i=0}^{M-1}t_{i,n+1}^{tt}-\sum_{i=0}^{M-1}t_{i,n-1}^{tt}}-C_i\right), \tag{45}$$

from which a generic error propagation scheme can be obtained:

This article has been accepted for publication in a future issue of this journal, but has not been fully edited. Content may change prior to final publication. Citation information: DOI 10.1109/TIM.2020.3033463, IEEE Transactions on Instrumentation and Measurement

$$\frac{\partial s_{i,n}}{\partial t_{i,n}^{tt}} = \frac{2\pi R}{\hat{T}_n}\frac{1}{2M}(2M-1), \quad \left.\frac{\partial s_{i,n}}{\partial t_{k,n}^{tt}}\right|_{k\neq i} = \frac{2\pi R}{\hat{T}_n}\frac{-1}{2M}, \quad \frac{\partial s_{i,n}}{\partial t_{i,n+1}^{tt}} = \frac{2\pi R}{\hat{T}_n}\left(-\frac{K_{i,n}}{2M}\right), \quad \frac{\partial s_{i,n}}{\partial t_{i,n-1}^{tt}} = \frac{2\pi R}{\hat{T}_n}\left(\frac{K_{i,n}-1}{2M}\right), \tag{46}$$

$$\delta s = \frac{2\pi R}{\hat{T}_n}\cdot\delta t^{tt}\sqrt{\frac{1}{2M}\left[K_i^2 - K_i + 2M - 1\right]} \approx \frac{2\pi R}{\hat{T}}\cdot\delta t^{tt}\sqrt{\frac{M-1}{M}}. \tag{47}$$

It is easy to note that, unless for the K_i which substitutes the C_i, the results is not changed, proving that the speed estimation does not affect the advantages of the improved technique.

The geometrical error related to the estimation of the C_i can also be computed for the tacho-less approach. Considering an average over N cycles, Eq. (33) is resumed

$$C_i = \frac{1}{N-2}\sum_{n=2}^{N-1}\frac{t_{i,n}^{tt} - \hat{t}_n^{tt}}{\hat{t}_{n+1}^{tt} - \hat{t}_n^{tt}}. \tag{48}$$

The C_i estimate will then be affected by an error which propagates from the time measurements. This can be obtained following the same scheme based on the averaged squared error. It is important to remember that M tip-timing times for the N cycles will be used in the computation of each C_i, so that $N\times M$ derivatives will have to be considered

$$\begin{aligned}\delta C_i^2 = {} & (N-4)\left(\frac{\partial C_i}{\partial t_{i,n}^{tt}}\delta t_C^{tt}\right)^2 + (N-4)(M-1)\left(\left.\frac{\partial C_i}{\partial t_{k,n}^{tt}}\right|_{k\neq i}\delta t_C^{tt}\right)^2 + M\left(\frac{\partial C_i}{\partial t_{i,1}^{tt}}\delta t_C^{tt}\right)^2 \\ & + \left(\frac{\partial C_i}{\partial t_{i,2}^{tt}}\delta t_C^{tt}\right)^2 + (M-1)\left(\left.\frac{\partial C_i}{\partial t_{k,2}^{tt}}\right|_{k\neq i}\delta t_C^{tt}\right)^2 + \left(\frac{\partial C_i}{\partial t_{i,N-1}^{tt}}\delta t_C^{tt}\right)^2 \\ & + (M-1)\left(\left.\frac{\partial C_i}{\partial t_{k,N-1}^{tt}}\right|_{k\neq i}\delta t_C^{tt}\right)^2 + M\left(\frac{\partial C_i}{\partial t_{i,N}^{tt}}\delta t_C^{tt}\right)^2\end{aligned} \tag{49}$$

So, computing the required partial derivatives, one can find the final formula

$$\delta C_i^2 = \delta t_C^{tt}\left(\frac{1}{T}\frac{1}{N-2}\right)^2\frac{1}{\sqrt{2M}}\left[2C_i^2 - 2C_i + 5 - 4M - 2N + 2MN\right], \tag{50}$$

and remembering that $3/4 \le C_i^2 - C_i + 1 \le 1$ for $0 < C_i < 1$, an approximation can be given as

$$\delta C_i^2 = \delta t_C^{tt}\left(\frac{1}{T}\frac{1}{N-2}\right)^2\frac{1}{2M}\left[5 - 4M + 2N(M-1)\right] \tag{51}$$

With $N \gg M$, the geometrical error finally results in

$$\delta C_i \approx \frac{1}{T}\frac{1}{N}\delta t_C^{tt}\frac{\sqrt{N(M-1)}}{\sqrt{M}} \approx \frac{1}{T}\frac{1}{\sqrt{N}}\delta t_C^{tt}. \tag{52}$$

The comparison between the traditional and the improved BTT is summarized in Tab. 1. It should be noted that, $\sqrt{\frac{M-1}{M}}$ is always lower than $\sqrt{2}$, so that the superiority the improved technique can be easily appreciated. Furthermore, bearing in mind that this work focuses on a large centrifugal compressor ($R/r \sim 10$, $M = 13$), the larger error contribution will come from

sensors vibrations. It is noteworthy that the improved BTT is insensitive to size effects, so that the propagation of such kind of error can be almost completely compensated.

Table 1
Comparison of measurement errors between the traditional and improved BTT in conditions with experimental uncertainties.

	Traditional BTT	Improved BTT
Resolution δt^r	$\delta s^r = \delta t^r \cdot 2\pi f R\sqrt{2K_i^2 - 2K_i + 2}$ $\delta s^r \approx \delta t^r \cdot 2\pi f R\sqrt{2}$	$\delta s^r = \delta t^r \cdot 2\pi f R\sqrt{\frac{1}{2M}\left[C_i^2 - C_i + 2M - 1\right]}$ $\delta s^r \approx \delta t^r \cdot 2\pi f R\sqrt{\frac{M-1}{M}}$
Sensors vibration δp	$\delta s^v = \delta p \cdot \sqrt{2}\frac{R}{r}\sqrt{\left(K_i^2 - K_i + \frac{1}{2}\left(1+\left(\frac{r}{R}\right)^2\right)\right)}$ $R/r \gg 1,\ \delta s^v \approx \delta p \cdot \sqrt{2}\frac{R}{r}\sqrt{\left(K_i^2 - K_i + \frac{1}{2}\right)}$ $R/r = 1$, *optimal case* $\delta s^v \approx \delta p \cdot \sqrt{2}$	$\delta s^v = \delta p\sqrt{\frac{1}{2M}\left[C_i^2 - C_i + 2M - 1\right]}$ $\delta s^v \approx \delta p\sqrt{\frac{M-1}{M}}$
Geometric δt_C	$\delta C_i \approx \delta t_C \frac{1}{T}\frac{1}{\sqrt{N}}\sqrt{2}$	$\delta C_i \approx \delta t_C \frac{1}{T}\frac{1}{\sqrt{N}}\frac{\sqrt{M-1}}{\sqrt{M}}$

5 The application of the improved BTT technique on centrifugal compressor blades

In order to demonstrate the superiority of test accuracy of the improved BTT technique with respect to the traditional method when applied for the condition monitoring and fault identification of large-scale centrifugal compressor blades, a centrifugal compressor test rig is used for the experimental verification. The test rig, shown by Fig. 11, consists of a motor, a coupler, a gearbox, an impeller, etc. The impeller is a semi-open one with 13 blades and 800 mm diameter designed to work with rotational speed ranging from 500rpm to 9000rpm. In order to simulate the blade failure which may occur in practical condition, a crack 70mm long is machined in one blade of the impeller, as shown in Fig. 12. When the compressor is working, the intake air flow of the compressor is controlled by an Inlet Guide Vane which allows controlling the flow rate in a wide range around the design value. In this paper, the vibration signal of the blades is sampled at 3 speeds of 4000rpm, 4500rpm and 5000rpm for 2 flow rates each, one according to the design value, and one smaller than it.

Before starting the measurement campaign, the calibration is performed in the best possible condition (low speed, reduced airflow disturbances). The thirteen blades are then named as 0, 1, ... ,12 as mentioned in section 2.2, so that blade 10 (physically the 11th blade) resulted to be the damaged one, as shown in Fig. 12 which also displays the installed sensors.

The BTT system used in this experiment consists of fiber optic sensors, a NI PCI high speed counter card, a BNC terminal block, and a photoelectric conversion box. In addition to this hardware, a Labview data acquisition software is designed using the C-DAQ platform. The arrival time series from both tip-timing and key-phase sensors are finally sampled in six conditions corresponding to three rotational speeds (4000rpm, 4500rpm and 5000rpm) for the two adjusted

air flows (design, smaller). In order to underline the superiority of the improved BTT technique, it is compared with the traditional technique to monitor blades vibration during the operation process of the compressor. The blades vibration estimated with the traditional technique (under 4000rpm and designed flow rate) is shown in Fig. 13 while the result based on the improved technique is displayed in Fig. 14. It is clearly seen that the proposed technique does not suffer from the abnormal trend which corrupts the traditional BTT results. In addition, in accordance to the theoretical analysis of sections 3 and 4, sources of experimental uncertainties will have more influence on the accuracy of the traditional technique resulting in more serious vibration amplitude deviations for blades with low and high indices i shown in Fig. 13(b). It can also be seen in Fig. 13(b) that the cracked blade could not be identified with the traditional BTT technique due to the effect of test errors. Therefore, the improved technique was further used in all operating conditions, producing the test results summarized in Tabs. 2, 3 and in Fig. 15.

Fig. 11. The centrifugal compressor test-rig.

Fig. 12. The installed sensors and impeller with cracked blade.

This article has been accepted for publication in a future issue of this journal, but has not been fully edited. Content may change prior to final publication. Citation information: DOI 10.1109/TIM.2020.3033463, IEEE Transactions on Instrumentation and Measurement

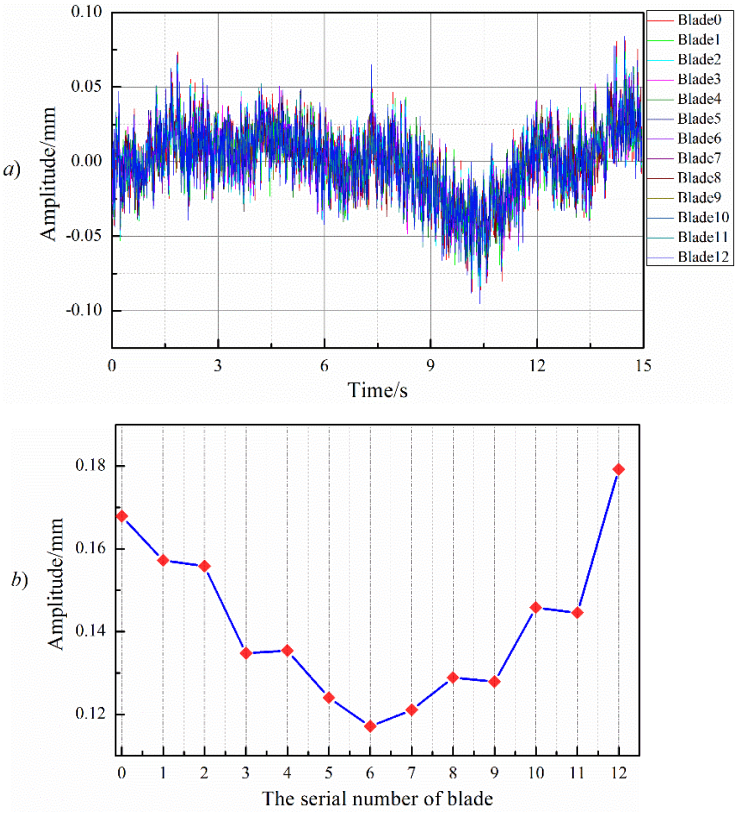

Fig. 13. (a) Vibration signal of each blade by referring to the key-phase signal. (b) Maximum peak to peak vibration amplitude of 0-12 blades.

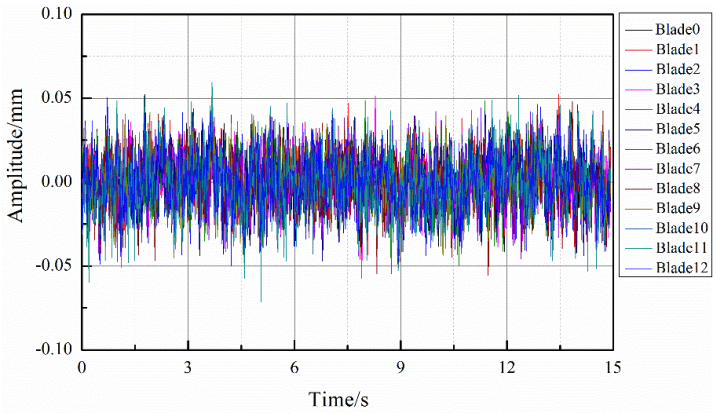

Fig. 14. Vibration amplitude of blades measured with the improved algorithm.

By comparing the vibration amplitude of each blade under the designed flow rate and small flow rate with different rotational speeds (shown in Tab. 2 and Tab. 3), which were obtained by the improved technique, it can be found that the vibration amplitude of most of the blades under small flow rate is larger than that under the designed flow rate. This phenomenon is reasonable, as the smaller flow rate condition is close to the surge point at which there exists obvious unsteady airflow pulsation. The generated unsteady aerodynamic load will then act on the blades leading to larger vibration amplitudes.

Besides, another important consideration regards the diagnostic ability of the method. As it can be noted from Tab. 3 and Fig. 18, the vibration amplitude of blade 10 is larger than the others, highlighting the cracked blade which can then be easily detected by the technique, guaranteeing

This article has been accepted for publication in a future issue of this journal, but has not been fully edited. Content may change prior to final publication. Citation information: DOI 10.1109/TIM.2020.3033463, IEEE Transactions on Instrumentation and Measurement

unambiguous results thanks to the improved accuracy. This is noteworthy as larger measurement error (e.g. traditional BTT sensors vibration deviations) could result in false vibration amplitude signals which may mask the cracked blade behavior leading to a wrong identification, as reported in Fig. 13(b).

Therefore, the improved algorithm proposed in this paper can be considered as an effective technique for large-scale centrifugal compressor condition monitoring and fault detection. A further dynamic analysis is conducted in the next section to demonstrate the relation among the damage and the abnormal blade vibration amplitude qualitatively.

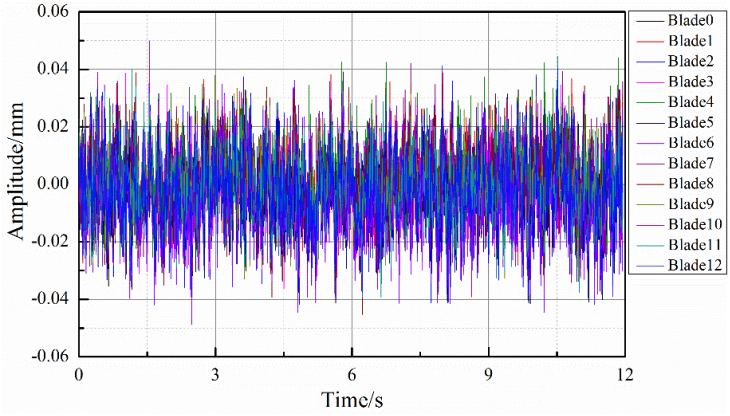

Fig. 15. Vibration amplitude of blades under 5000rpm and design flow rate.

Table 2. Maximum peak to peak vibration amplitude of blade 0-6, (unit mm)

Operational condition	Blade 0	Blade 1	Blade 2	Blade 3	Blade 4	Blade 5	Blade 6
4000rpm Designed flow rate	0.0612	0.0700	0.0670	0.0669	0.0613	0.0650	0.0667
4000rpm Low flow rate	0.0677	0.0763	0.0762	0.0759	0.0735	0.0744	0.0815
4500rpm Designed flow rate	0.0836	0.0809	0.0741	0.0744	0.0890	0.0791	0.0859
4500rpm Low flow rate	0.0838	0.0878	0.0912	0.0863	0.081	0.0780	0.0805
5000rpm Designed flow rate	0.0846	0.0955	0.0922	0.0897	0.0965	0.0869	0.0836
5000rpm Low flow rate	0.0925	0.0906	0.0939	0.0824	0.0906	0.0872	0.0916

Table 3. Maximum peak to peak vibration amplitude of blade 7-12, (unit mm)

Operational condition	Blade 7	Blade 8	Blade 9	**Blade 10**	Blade 11	Blade 12
4000rpm Designed flow rate	0.0639	0.0594	0.0686	**0.0752**	0.0553	0.0664
4000rpm Low flow rate	0.0780	0.0682	0.0731	**0.0884**	0.0791	0.0776
4500rpm Designed flow rate	0.0829	0.0746	0.0851	**0.0929**	0.0861	0.0921
4500rpm Low flow rate	0.0767	0.0728	0.0860	**0.1015**	0.0925	0.0812
5000rpm Designed flow rate	0.0807	0.0805	0.0842	**0.0987**	0.0902	0.0926
5000rpm Low flow rate	0.0890	0.08490	0.0913	**0.1090**	0.0917	0.0807

6 Dynamic analysis for experimental result

According to the obtained experimental results under different working conditions, the faulted blade is found to have larger vibration amplitude than the other blades as mentioned above. In order to justify this finding, a lumped-parameter-model is built according to Ref. [25] to conduct a simplified analysis considering the effect of crack on the blade vibration amplitude. Limited to the length of this paper, the vibration amplitude difference between the cracked blade and normal blades is analyzed qualitatively. Each blade is considered as a lumped-parameter-model with single degree of freedom, where the equivalent mass of a blade is set as m_i, the equivalent stiffness is k_i and the equivalent damping is c_i, with $i = 0,1...M-1$. In addition, the equivalent coupling stiffness between two adjacent blades is given as k_{cp}. The forced vibration of each blade under the excitation of the fluid can then be approximated with this simplified model by solving a system of 13 equations reported in Eq. (53), coming from the free body analysis of each mass

$$\begin{cases} m_0\ddot{x}_0 + c_0\dot{x}_0 + k_0x_0 + k_{cp}(x_0 - x_{12}) + k_{cp}(x_0 - x_1) = F_0 \\ \quad\quad ... \quad ... \\ m_i\ddot{x}_i + c_i\dot{x}_i + k_ix_i + k_{cp}(x_i - x_{i-1}) + k_{cp}(x_i - x_{i+1}) = F_i \\ \quad\quad ... \quad ... \\ m_{12}\ddot{x}_{12} + c_{12}\dot{x}_{12} + k_{12}x_{12} + k_{cp}(x_{12} - x_{11}) + k_{cp}(x_{12} - x_0) = F_{12} \end{cases} . \tag{53}$$

The above system of equations can be rewritten in matrix form as

$$\mathrm{M}\ddot{\mathrm{X}} + \mathrm{C}\dot{\mathrm{X}} + \mathrm{K}\mathrm{X} = \mathrm{F} . \tag{54}$$

The main issue is now related to the parameter estimation. The blade mass m_i and the stiffness k_i can be evaluated by referring to Refs. [26-27]. It is relevant to underline that the actual blade stiffness will vary during different operational conditions due to the dynamic effects as a function of the speed. Furthermore each blade could theoretically show a different stiffness due to manufacturing error, operation wear and so on, so that a mistuning factor δ_i can be introduced for each blade, leading to a final stiffness of $k_i^d = (1+\delta_i)k_i(\omega)$, $\delta_i < 1$. Regarding the coupling stiffness, in general it is not set independently, but is usually given as a fraction of the blade stiffness, according to the relation $k_j = Pk_i$, where P is the coupling factor.

Focusing on the cracked blade (blade 10) shown by Fig. 16, its stiffness could be in first approximation modelled with a reduced value $k_{iop} < k_i^d$, which corresponds to the stiffness of the faulted blade when the crack is fully open. During the blade vibration, the crack will open and close periodically so that, identifying with $k_{icls} \simeq k_i^d$ the stiffness of the blade when the crack is fully closed, one can write, according to Ref. [26]

This article has been accepted for publication in a future issue of this journal, but has not been fully edited. Content may change prior to final publication. Citation information: DOI 10.1109/TIM.2020.3033463, IEEE Transactions on Instrumentation and Measurement

$$k_i^{eq}(t) = k_{iop} + \frac{1}{2}(k_{icls} - k_{iop})(1 + \cos(\omega t)), \tag{55}$$

where the angular frequency ω is related to the fluid excitation. The natural frequency ω_{n_i} and modal shapes φ_i of the blades can then be calculated for the undamped free case as in Ref. [28], both for the healthy and damaged condition.

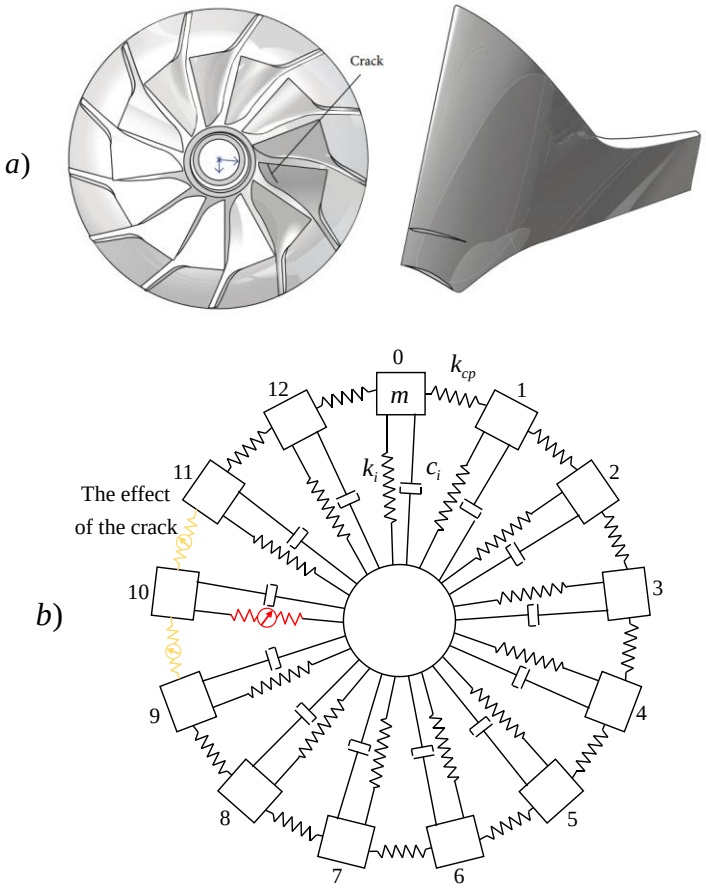

Fig. 16. Model of impeller with a cracked blade: (a) Three-dimensional model for the faulted impeller. (b) Simplified dynamic model of the faulted impeller.

The forced vibration response of the cracked blade under fluid excitation is then studied, considering a periodic excitation, an assumption that is likely to be verified in case of a stationary flow field [25,29,30].

The i-th blade forcing term, F_i, can be expressed as follows:

$$F_i = F_0 \cos(\Omega t + 2\pi E(i-1)/n), \tag{56}$$

where, F_0 is the amplitude of the fluid excitation force, Ω is the impeller rotational speed in rad/s, E is the order of the airflow force which is set as 1 and $2\pi E(i-1)/n$ accounts for

This article has been accepted for publication in a future issue of this journal, but has not been fully edited. Content may change prior to final publication. Citation information: DOI 10.1109/TIM.2020.3033463, IEEE Transactions on Instrumentation and Measurement

the phase in the excitation of each single blade (blades are supposed to be equispaced).

Considering the effect of damping $c_i = 2\xi m_i \omega_n$ where ξ is the damping ratio, the damped, forced vibration response of the blade can be finally obtained [25,31]. As a simplified qualitative study, reasonable, physically consistent values were assigned to the parameters to simulate a generic compressor scale model. Considering a 20% reduction for the open crack stiffness and a small mistuning of the order of 1%, the vibration amplitude for each blade can be found in both the healthy and damaged case. In Fig. 17 the blades vibration amplitudes for the damaged case are reported so as to highlight the substantial increase of the order of 25% induced by the presence of the crack. In order to compare the simulation result to the experimental results, Fig. 18 reports the measured blade vibration amplitude for the centrifugal compressor at 5000rpm. As expected, the two trends are compatible, confirming the goodness of the improved BTT technique in diagnosing possible cracks with an increased accuracy and reliability for large-scale centrifugal compressor blades.

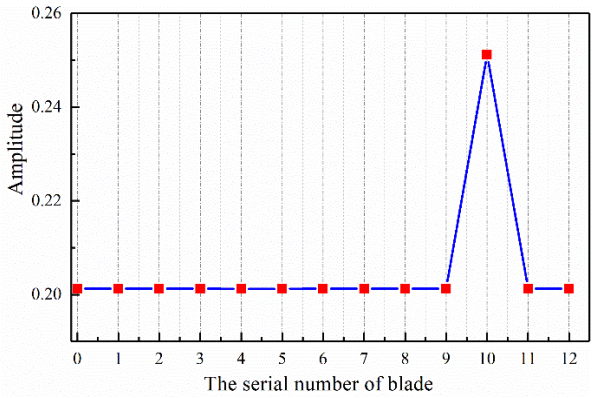

Fig. 17. Simulation result for vibration amplitude of blades.

Fig. 18. Measured vibration amplitude of blades under 5000rpm with small flow rate.

7 Conclusions

The reliability of BTT technique in experimental applications was tested in this paper for a large-scale centrifugal compressor. The complexity of the working conditions and the various sources of errors can in fact strongly affect the BTT results, compromising its diagnostic ability. The effect of the main sources of errors has been investigated in detail by using uncertainty analysis, thus underlining the traditional BTT weaknesses. An improved BTT technique has then been proposed, in particular to compensate for the effect of the sensor vibration, which can be

predominant in the case of large machines. To experimentally verify the effectiveness of this improved technique, many tests were conducted on a large compressor with a cracked blade. The results have shown that the improved technique outperforms the traditional one in terms of accuracy and reliability of the diagnosis of the cracked blade, whose abnormal vibration have been easily and reliably detected under different rotational speeds and flow rates. Based on this experimental evidence, a dynamic model has been built to provide a proof of the easily perceivable correlation among the cracked blade and the larger vibration amplitudes.

Currently, most of the research works about BTT are focused on straight blades rotating machinery such as axial flow fans, aero engines, etc. Despite the similarity of these machines and the centrifugal compressors, little reference can be found about the condition monitoring of large-scale centrifugal compressor blades, because of the more complex flow field and the more nonstationary conditions which usually leads to inaccurate results. The improved BTT technique here introduced, aims to fill this gap, demonstrating to be suitable for large-scale machines, outperforming traditional BTT technique. This improved technique can better estimate the blades vibration, proving its appropriateness for an improved on-line condition monitoring of any turbomachinery.

Acknowledgements: The work was supported by the Natural Science Foundation of China under Grant No. 51575075 and China Scholarship Council (No. 201706060161).

References

[1] C.B. He, H.K. Li, X.W. Zhao, "Weak characteristic determination for blade crack of centrifugal compressors based on underdetermined blind source separation," *Measurement*, vol. 128, pp. 545-557, 2018.

[2] S.M. Wu, Z.K. Wang, H.Q. Li, Z.B. Yang, S.H. Tian, R.Q. Yan, X.F. Chen, "A hybrid fault diagnosis approach for blade crack detection using blade tip timing," in *2020 IEEE International Instrumentation and Measurement Technology Conference (I2MTC).* IEEE, 2020, pp. 1-5.

[3] J. Zeng, K.K. Chen, H. Ma, T.T. Duan, B.C. Wen, "Vibration response analysis of a cracked rotating compressor blade during run-up process," *Mechanical Systems and Signal Processing*, vol. 118, pp. 568-583, 2019.

[4] H. Ma, Y. Lu, Z. Wu, X. Tai, H. Li, B. Wen, "A new dynamic model of rotor–blade systems," *Journal of Sound and Vibration*, vol. 357, pp. 168-194, 2015.

[5] H.L. Xu, Z.S. Chen, Y.M. Yang, L.M. Tao, "Effects of crack on modal parameters of mistuned blades," in *2016 Prognostics and System Health Management Conference*. IEEE, 2016, pp. 1-6.

[6] Z.K. Wang, Z.B. Yang, S.M. Wu, H.Q. Li, S.H. Tian, X.F. Chen, "An improved multiple signal classification for non-uniform sampling in blade tip timing," *IEEE Transactions on Instrumentation and Measurement* (*Early Access*), 2020.

[7] G. Battiato, C.M. Firrone, T.M. Berruti. "Forced response of rotating bladed disks: Blade Tip-Timing measurements," *Mechanical Systems and Signal Processing*, vol. 85, pp. 912-926, 2017.

[8] Z.K. Wang, Z.B. Yang, S.M. Wu, H.Q. Li, R.Q. Yan, S.H. Tian, X.W. Zhang, X.F. Chen, "An OPR-free blade tip timing method based on blade spacing change," in 2020 *IEEE International Instrumentation and Measurement Technology Conference (I2MTC).* IEEE, 2020, pp. 1-5.

[9] W.M. Wang, D.F. Hu, Q.H. Li, X.L. Zhang, "An improved non-contact dynamic stress measurement method for turbomachinery rotating blades based on fundamental mistuning model," *Mechanical Systems and Signal Processing*, vol. 145, pp. 1-18, 2020.

[10] P. Procházka, F. Vaněk, "New methods of noncontact sensing of blade vibrations and deflections in turbomachinery," *IEEE Transactions on Instrumentation and Measurement*, vol. 63, pp. 1583-1592, 2014.

[11] S. Heath, M. Imregun, "An improved single-parameter tip-timing method for turbomachinery blade vibration measurements using optical laser probes," *International Journal of Mechanical Sciences*, vol. 38, pp. 1047-1058, 1996.

[12] S. Heath, M. Imregun, "A Survey of blade tip-timing measurement techniques for turbomachinery vibration," *Journal of Engineering for Gas Turbines and Power-Transactions of the ASME*, vol. 120, pp. 784-791, 1998.

[13] I.B. Carrington, J.R. Wright, J.E. Cooper, G. Dimitriadis, "A comparison of blade tip-timing data analysis methods," *Proceedings of the Institution of Mechanical Engineers, Part G: Journal of Aerospace Engineering*, vol. 215, pp. 501-512, 2001.

[14] W.M. Wang, S.Q. Ren, S. Huang, Q.H. Li, K. Chen, "New step to improve the accuracy of blade synchronous vibration parameters identification based on combination of GARIV and LM algorithm," in *Proceedings of ASME Turbo Expo 2017: Turbomachinery Technical Conference and Exposition*, American Society of Mechanical Engineers, 2017, pp. 1-10.

[15] H.T. Guo, F.J. Duan, J.L. Zhang, "Blade resonance parameter identification based on tip-timing method without the once-per revolution sensor," *Mechanical Systems and Signal Processing*, vol. 66-67, pp. 625-639, 2016.

[16] S.M. Wu, Z.B. Zhao, Z.B. Yang, S.H. Tian, L.H. Yang, X.F. Chen, "Physical constraints fused equiangular tight frame method for Blade Tip Timing sensor arrangement," *Measurement*, vol. 145, pp. 841-851, 2019.

[17] Z. Hu, J. Lin, Z. Chen, Y. Yang, "A non-uniformly under-sampled blade tip-timing signal reconstruction method for blade vibration monitoring," *Sensors*, vol. 15, pp. 2419-2437, 2015.

[18] J. Lin, Z. Hu, Z.S. Cheng, Y.M. Yang, H.L. Xu, "Sparse reconstruction of blade tip-timing signals for multi-mode blade vibration monitoring," *Mechanical Systems and Signal Processing*, vol. 81, pp. 250-258, 2016.

[19] M.H. Pan, Y.M. Yang, F.J. Guan, H.F. Xu, H.L. Xu, "Sparse representation based on frequency detection and uncertainty reduction in blade tip timing measurement for multi-mode blade vibration monitoring," *Sensors*, vol. 17, pp. 1745–1764, 2017.

[20] S.M. Wu, P. Russhard, R.Q. Yan, S.H. Tian, S.B. Wang, Z.B. Zhao, X.F. Chen, "An adaptive online blade health monitoring method: from raw data to parameters identification," *IEEE Transactions on Instrumentation and Measurement*, vol. 69, pp. 2581-2592, 2020.

[21] P. Russhard, "Blade tip timing (BTT)," *AIP Conference Proceedings*, vol. 1740, pp. 1-13, 2016.

[22] G. Rossi, J.F. Brouckaert, "Design of blade tip timing measurements systems based on uncertainty analysis," *58th International Instrumentation Symposium*, 2020, pp. 4-8.

[23] B. Salhi, J. Lardiè, M. Berthillier, P. Voinis, C. Bodel, "Modal parameter identification of mistuned bladed disks using tip timing data," *Journal of Sound and Vibration*, vol. 314, pp. 885-906, 2008.

[24] K. Chen, W.M. Wang, X.L. Zhang, Y. Zhang, "New step to improve the accuracy of blade tip timing method without once per revolution," *Mechanical Systems and Signal Processing*, vol. 134:106321, 2019.

[25] H.L. Xu, Z.S. Chen, Y.M. Yang, L.M. Tao, X.F. Chen, "Effects of crack on vibration characteristics of mistuned rotated blades," *Shock and Vibration*, vol. 2017, pp. 1-18, 2017.

[26] S.M. Cheng, A.S.J. Swamidas, X.J. Wu, W. Wallace, "Vibrational response of a beam with a breathing crack," *Journal of Sound and Vibration*, vol. 225, pp. 201-208, 1999.

[27] H.L. Xu, Z.S. Chen, Y.P. Xiong, Y.M. Yang, L.M. Tao, "Nonlinear dynamic behaviors of rotated blades with small breathing cracks based on vibration power flow analysis," *Shock and Vibration*, vol. 2016, pp. 1-12, 2016.

[28] T.G. Chondros, A.D. Dimarogonas, J. Yao, "Vibration of a beam with a breathing crack," *Journal of Sound and Vibration*, vol. 239, pp. 57-67, 2001.

[29] T. Miyakozawa, R.E. Kielb, K.C. Hall, "The effects of aerodynamic asymmetric perturbations on forced response of bladed disks," *Journal of Turbomachinery*, vol. 131, pp. 1-8, 2009.

[30] J.A. Beck, J.A. Justice, O. Scott-Emuakpor, T.J. George, J.M. Brown, "Next generation traveling-wave excitation system for integrally bladed rotors," *Journal of Aerospace Engineering*, vol. 28, pp. 1-12, 2015.

[31] Q.K. Han, J.Y. Zhai, H. Zhang, "Fundamentals of mechanical dynamics and its simulation methods," *Wuhan: Wuhan University of Technology Press*, 2017.